Photodetachment of free hexahalogenometallate doubly charged anions in the gas phase: $[ML_6]^{2-}$, (M=Re, Os, Ir, Pt; L=Cl and Br)

Xue-Bin Wang and Lai-Sheng Wang
Department of Physics, Washington State University, Richland, Washington 99352 and W. R. Wiley Environmental Molecular Sciences Laboratory, Pacific Northwest National Laboratory, Richland, Washington 99352

(Received 29 April 1999; accepted 15 June 1999)

We report the first observation and photodetachment photoelectron spectroscopic study of a series of hexahalogenometallates dianions MCl_6^{2-} (M=Re, Os, Ir, and Pt) and MBr_6^{2-} (M=Re, Ir, and Pt) in the gas phase. All of these species were found to be stable as free gaseous doubly charged anions. Photoelectron spectra of all the dianions were obtained at several detachment photon energies. The photon-energy-dependent spectra clearly revealed the dianion nature of these species and allowed the repulsive Coulomb barriers to be estimated. The binding energies of the second excess electron in MCl_6^{2-} (M=Re, Os, Ir, Pt) were determined to be 0.46 (5), 0.46 (5), 0.82 (5), and 1.58 (5) eV, respectively, and those in MBr_6^{2-} (M=Re, Ir, Pt) to be 0.76 (6), 0.96 (6), and 1.52 (6) eV, respectively. A wealth of electronic structure information about these metal complexes were obtained and low-lying and highly-excited electronic states of the corresponding singly charged anions were observed. Detachment from metal *d* orbitals or ligand orbitals were observed and could be clearly distinguished; detachments from the metal *d*-orbitals all occur at low binding energies whereas those from the ligand-dominated orbitals all take place at rather high binding energies. We also found a remarkable correlation between electron affinities measured *in vacuo* and the redox potentials obtained in the solution phase of these species. © *1999 American Institute of Physics.* [S0021-9606(99)00234-2]

I. INTRODUCTION

Multiply charged anions (MCAs) are common in solutions and solids, but are challenging to study in the gas phase both experimentally and theoretically.[1] Strong Coulomb repulsion between the excess negative charges makes MCAs difficult to be formed in the gas phase whereas strong electron correlation effects and the diffuse nature of the excess charges make theoretical investigations rather difficult. Therefore, despite of their ubiquity and importance in the condensed phases, our knowledge about MCAs are still scarce.[1–5]

Theoretical search of small stable MCAs has been very active recently[6–26] and has been reviewed by Scheller *et al.*[1] As discussed by Boldyrev, Gutowski, and Simons,[3] there are three types of stability of MCAs. The first is their electronic stability. If A^{n-} at its own optimal geometry is more stable than $A^{(n-1)-}$ at the same geometry, it is vertically electronically stable. If A^{n-} at its optimal geometry is more stable than $A^{(n-1)-}$ at its own optimal geometry, A^{n-} is adiabatically electronically stable. Second, if A^{n-} has all real vibrational frequencies at its optimal geometry, it is locally geometrically stable. Finally, if A^{n-} is more stable than any possible dissociation fragment, it is thermodynamically stable. There is a consensus currently that all free atoms cannot support two or more extra electrons because of the enormous Coulomb repulsion. It is also concluded that all isolated diatomic or triatomic dianions are not stable,[3] although they may exist as resonance or metastable excited species.[25–27] For larger systems (more than four atoms), Sheller and Cederbaum predicted some electronically stable MCAs consisting of halogen-type ligands and a metal atom (e.g., LiF_3^{2-}, NaF_3^{2-}, KF_3^{2-}),[8–13] although these dianions are not stable thermodynamically. Cederbaum and co-workers have also proposed a ''construction principle'' to form stable gaseous MCAs based on the alkali–halogen systems.[16,17] Many common MCAs known to exist in the condensed phases, such as CO_3^{2-}, SO_4^{2-}, SeO_4^{2-}, and PO_4^{3-}, are found electronically unstable in the gas phase.[8,14] Gutowski *et al.* studied the local and electronic stability of several octahedral closed-shell $[MF_6]^{n-}$ MCAs containing early $4d$ and $5d$ transition metals.[20,22] Some of these MCAs are predicted to be stable locally and electronically (vertically). Miyoshi and Sakai predicted CrF_6^{2-} and MoF_6^{2-} to be electronically stable with octahedral geometry.[28]

Experimental study of MCAs has also made progress recently. A number of dianions have been observed in the gas phase using mass spectrometry and has been well reviewed.[1–5] Lately, Compton and co-workers have observed and investigated dianions of several fullerenes and fullerene derivatives.[29–31] As demonstrated by Kebarle and co-workers,[32] electrospray ionization (ESI) (Ref. 33) is an ideal technique to produce gas phase MCAs; and many more MCAs have been observed using the ESI technique, including fullerenes and derivatives as well as small organic and inorganic species.[34–36]

Recently, we have developed an experimental technique to investigate gas phase multiply charged anions using photodetachment photoelectron spectroscopy (PES) and an ESI source.[37–42] PES is particularly ideal to probe the intrinsic

properties of free multiply charged anions and directly yields information about their electronic stability, intramolecular Coulomb repulsion, and solvation effects, as we have shown in our investigations of the citric acid dianion,[38] a series of linear dicarboxylate dianions $[O_2C(CH_2)_nCO_2^-$ $(n=2-12)]$,[39,40] $S_2O_8^{2-}$,[41] and $(MSO_4)_2^{2-}$ (M=Na,*K*) dianions.[42]We have observed directly the repulsive Coulomb barrier (RCB), that exists in any multiply charged anion against electron detachment.[1,3,5] Particularly, we found that the RCB is equal in magnitude to the intramolecular Coulomb repulsion between the two excess charges. The effects of the RCB on the PES spectra and electron tunneling through the RCB have also been observed.[38–43] In addition to information about their electronic stability, PES spectra also provide electronic structure information about the MCAs. Due to the relatively long time scale of our experiment (~0.1s), any MCAs that we observe should have at least local and thermodynamical stabilities with a sufficiently long lifetime of at least ~0.1s.

Our motivation to search and probe the properties of MCAs led us to consider the octahedral or quasioctahedral hexahalogenometallates dianions, MX_6^{2-} (M=Re, Os, Ir, and Pt, X=Cl, Br) in the present investigation. These dianions are classical Werner-type transition metal complexes[44] and are commonly found as constituents of solids, melts, and solutions.[45] These species are interesting electron transfer agents in solutions and have been extensively studied as such.[46–51] There is also an extensive body of literature on the properties of these species in solids. Their ground state electronic energy levels have been investigated in numerous studies of optical absorption,[52] magnetic circular dichroism,[53] and x-ray photoelectron spectroscopy.[54] Their geometry structures in crystals have been determined.[55] There have also been several theoretical investigations about the electronic and geometrical structures of these hexahalogenometallates.[56–58] To the best of our knowledge, there is no gas phase study on these species and it is not known if they are stable as free dianions or can be formed in the gas phase.

Gas phase studies of these species would be interesting in at least three aspects. First, from the point of view of MCAs, it would be important to understand their electronic and thermodynamic stability in the gas phase. Second, the electronic structure information obtained through PES would be valuable to compare to theoretical calculations, which are often done on gaseous species and used to understand properties of the condensed phases. Third, photodetachment is the simplest oxidation reaction. It would be interesting to compare the gas phase electron binding energies of these species to their redox potentials in solutions.

In this paper, we present the first and a systematic PES study of several MCl_6^{2-} (M=Re, Os, Ir, and Pt) and MBr_6^{2-} (M=Re, Ir, and Pt) dianions in the gas phase at four photon energies; 532 nm (2.331 eV), 355 nm (3.496 eV), 266 nm (4.661 eV), and 193 nm (6.424 eV). We show that these late 5*d* transition metal hexacholoride and bromide dianions are indeed stable in the gas phase both electronically and thermodynamically—all the dianions possess positive electron binding energies. Well-resolved detachment features were obtained in the PES spectra of all the species, yielding a wealth of electronic structure information about both the dianions and the singly charged species. Detachment from the central metal *d*-orbitals and ligand orbitals were clearly observed and distinguished. PES spectra measured at different photon energies clearly revealed the doubly charged nature of these species and allowed the RCB to be estimated. In addition, we found a remarkable correlation between the electron binding energies measured *in vacuo* and the redox potentials obtained in solutions.

II. EXPERIMENTS

The experiments were performed with a magnetic-bottle time-of-flight (TOF) PES apparatus coupled to an ESI source. Details of the experiments have been published elsewhere[37] and only a very brief description is given here. A 10^{-3} M solution of each salt K_2ML_6 (M=Re, Os, Ir, Pt; L=Cl, Br) (*p*H~7) in a water/methanol (2/98 ratio) mixed solvent was sprayed through a 0.01 mm inner diameter syringe needle (biased at −2.2 kV) into ambient atmosphere. The resulting charged droplets were fed into a desolvation capillary heated to ~70 °C. Molecular anions formed in the desolvation capillary were guided by a radio-frequency quadruple ion-guide into a 3D quadruple ion-trap, where ions were accumulated for 0.1 s before being pulsed out into the extraction zone of a TOF mass spectrometer. The dominating anion signals in each case were the ML_6^{2-} dianions, which were mass-gated and decelerated before intercepted by a probe laser beam in the photodetachment zone of the magnetic-bottle photoelectron analyzer. Both an ArF excimer laser (193 nm) and a Nd:YAG laser (532, 355, and 266 nm) were used for photodetachment. The experiments were done at 20 Hz with the ion beam off at alternating laser shots for background substraction. Photoelectrons were collected at nearly 100% efficiency by the magnetic-bottle and analyzed in a 4 m long electron flight tube. Photoelectron TOF spectra were collected and then converted to kinetic energy spectra, calibrated by the known spectra of I^- and O^-. The electron binding energy (BE) spectra presented were obtained by subtracting the kinetic energy spectra from the detachment photon energies. The electron kinetic energy resolution was $\Delta E/E \sim 2\%$, i.e., 20 meV for 1 eV kinetic energy electrons.

III. RESULTS

Figure 1 shows the PES spectra of MCl_6^{2-} (M=Re, Os, Ir, and Pt) at 193 nm. All the spectra exhibit rich and well resolved features, as labeled, which represent transitions from the electronic ground state of the dianions to the ground and excited states of the corresponding singly charged anions. Using the single-electron picture (Koopmans' theorem), these PES features can be alternatively viewed as removing electrons from the occupied molecular orbitals (MOs) of the dianions. The second electron binding energies of the MCl_6^{2-} dianions (M=Re, Os, Ir, and Pt), determined from the threshold of the *X* feature in each spectrum, are 0.46, 0.46, 0.82, and 1.58 eV, respectively. Overall, the spectra of $ReCl_6^{2-}$ and $PtCl_6^{2-}$ appear to be less congested than

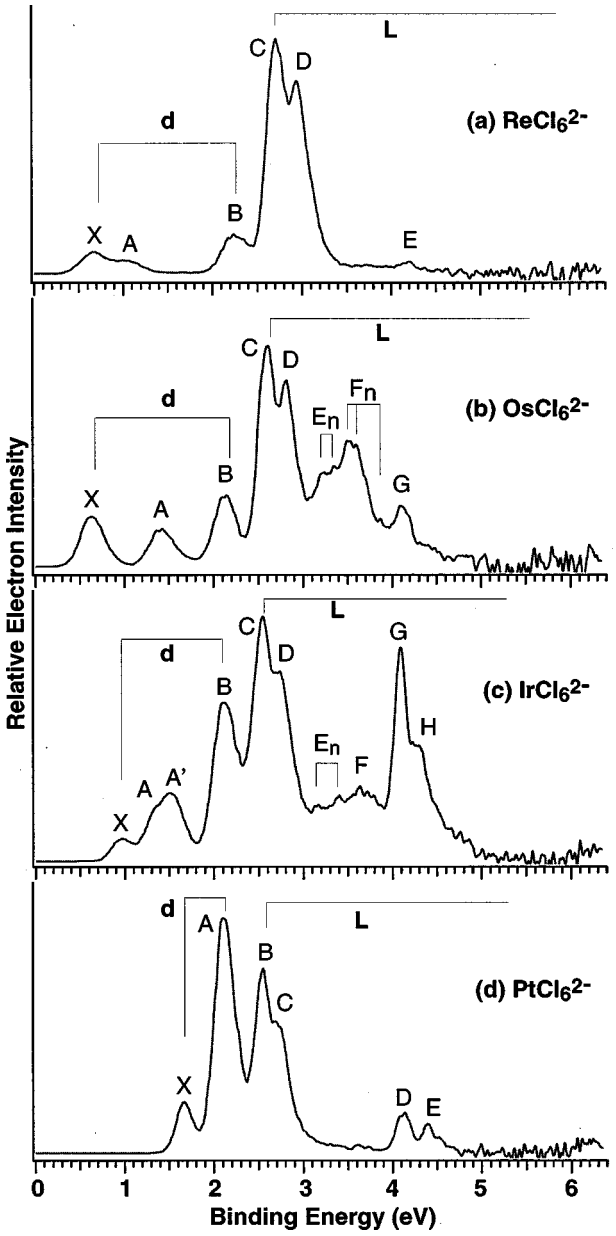

FIG. 1. Photoelectron spectra of MCl_6^{2-} (M=Re, Ir, Os, and Pt) at 193 nm. The labels '*d*' and '*L*' indicate features from metal *d*-orbitals and ligand-orbitals, respectively.

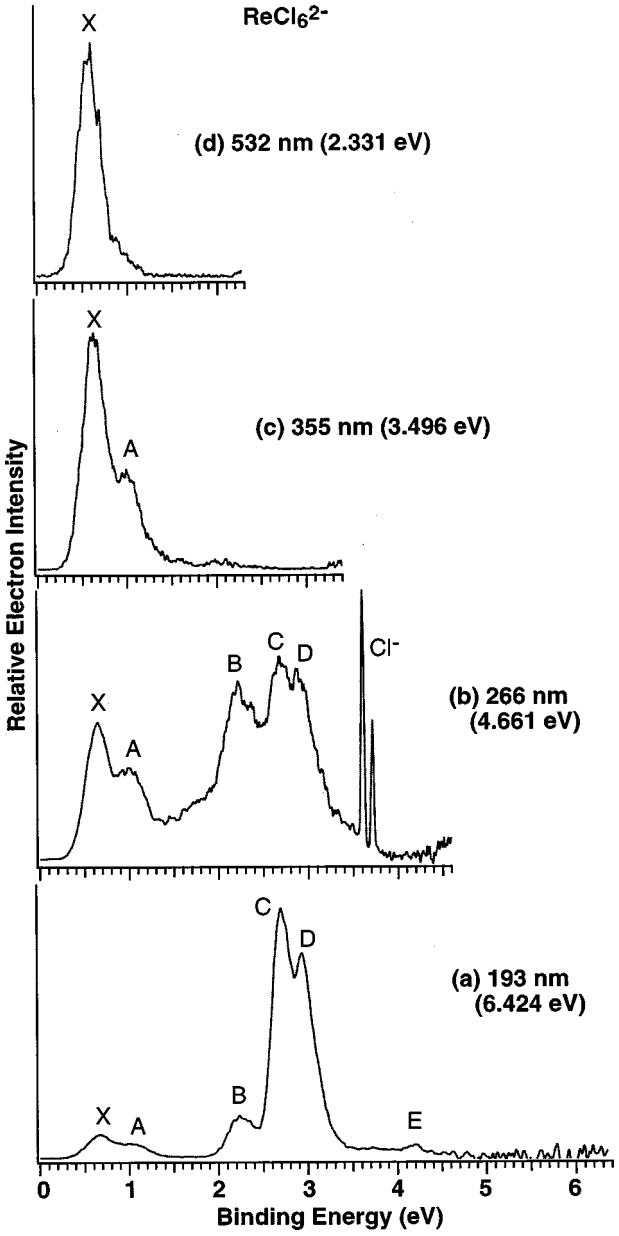

FIG. 2. Photoelectron spectra of $ReCl_6^{2-}$ at (a) 193 nm, (b) 266 nm, (c) 355 nm, and (d) 532 nm.

that of $OsCl_6^{2-}$ and $IrCl_6^{2-}$. It is also worth to note that there are no spectral features at higher BEs ($\gtrsim$4.5 eV) in all the spectra.

The BEs and spacings of the first few spectral features (*X*, *A*, and *B* for Re, Os, and Ir; X and A for Pt) are different in each spectrum, depending on the central metal atoms. These lower BE features also appeared to have relatively low intensities except for the *B* feature in $IrCl_6^{2-}$ [Fig. 1(c)] and the *A* feature in $PtCl_6^{2-}$ [Fig. 1(d)]. Each spectrum showed a similar and prominent doublet feature between 2.5 and 3.0 eV [*C* and *D* in Figs. 1(a)–1(c); B and C in Fig. 1(d)]. There also appeared to be another similar doublet feature between 4.0–4.5 eV in each spectrum although they were less definitive in Figs. 1(a) and 1(b). These similar spectral features among the four complexes were indications that they were due to detachment from the ligand-derived MOs whereas the lower BE features, which vary according to the metals, are due to detachment from the metal *d*-orbitals, as labeled in Fig. 1 (''*d*'' for *d*-orbitals; ''*L*'' for ligands). As shown below, these assignments were supported by the data on the bromide complexes.

Photon-energy-dependent spectra for MCl_6^{2-} (M=Re, Os, Ir, and Pt) are shown in Figs. 2–5, respectively. The disappearance of the high *BE* features (although thermodynamically possible) in the lower photon energy spectra was a direct consequence of the RCB in MCAs. From these data the barrier height for each dianion was estimated, as discussed below. The sharp peaks in each 266 nm spectrum was due to Cl^- as a result of photodissociation of the parent dianions and subsequent photodetachment by a second photon. Very weak signals due to Cl^- were discernible in the

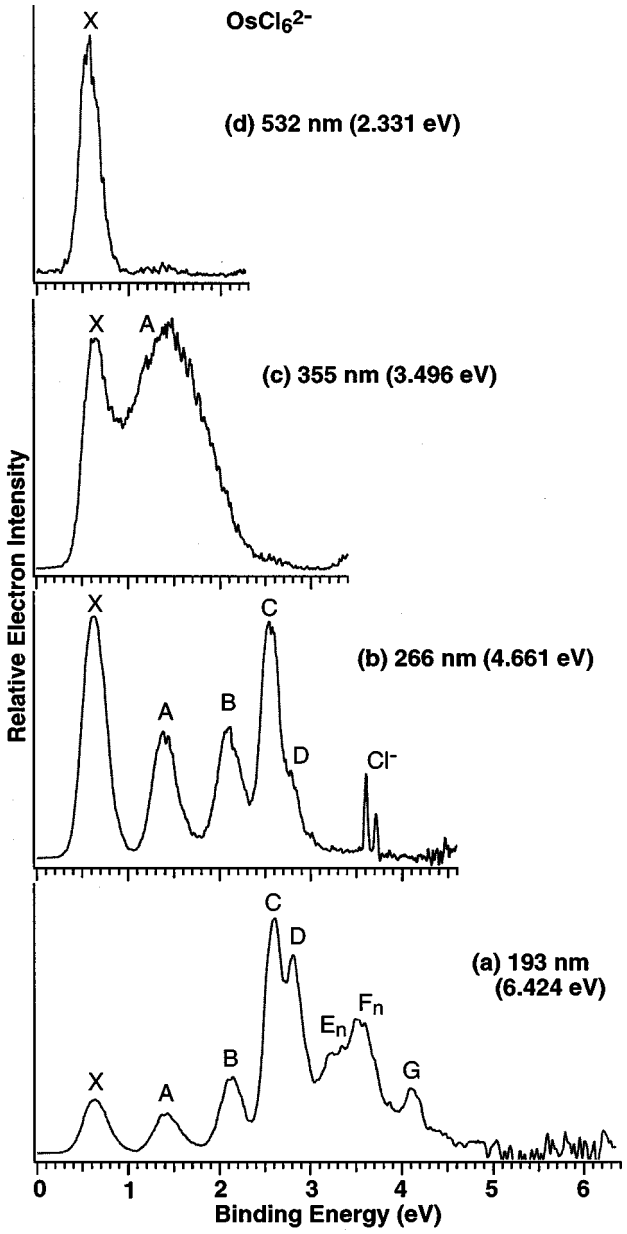

FIG. 3. Photoelectron spectra of $OsCl_6^{2-}$ at (a) 193 nm, (b) 266 nm, (c) 355 nm, and (d) 532 nm.

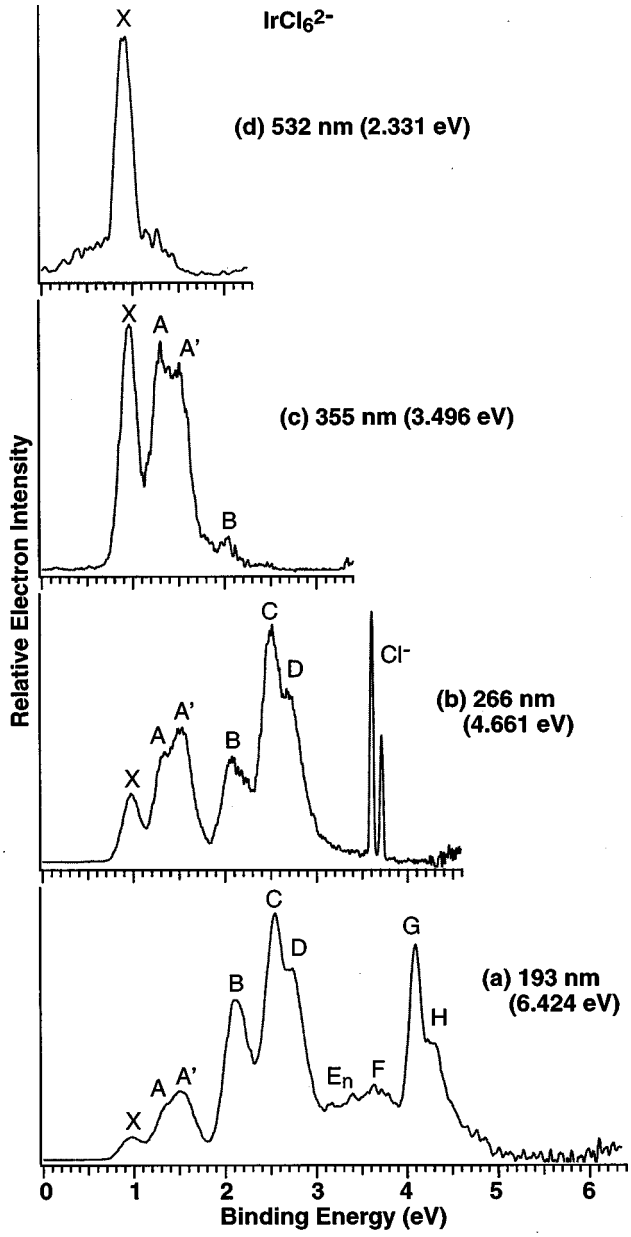

FIG. 4. Photoelectron spectra of $IrCl_6^{2-}$ at (a) 193 nm, (b) 266 nm, (c) 355 nm, and (d) 532 nm.

193 nm spectrum of $PtCl_6^{2-}$, as well [Fig. 5(a)].

Figures 6–8 show the PES spectra of MBr_6^{2-} at 266 and 193 nm for M=Re, Ir, and Pt, respectively, along with the corresponding MCl_6^{2-} spectra for comparison. As expected, the spectral features of the bromide complexes were similar to those of the chlorides and there was a one-to-one correspondence between the features of the chlorides and the bromides, as labeled in Figs. 6–8. The similar patterns and relative intensities of the first few low BE features between the chlorides and the bromides were consistent with the above identification of their being from the central metal *d*-orbitals. The anticipated larger separation of the doublet peaks, in the bromides (*C*/*D* for Re and Ir; *B*/*C* and *D*/*E* for Pt; *G*/*H* for Ir) confirmed their ligand origins. The significant enhancement of the *E* feature in $ReBr_6^{2-}$ (Fig. 6), compared to that in $ReCl_6^{2-}$, was due to its slightly lower BE and RCB, as discussed below. The second electron binding energies of MBr_6^{2-} were measured from the threshold of the *X* bands from each PES spectra to be 0.76, 0.96, and 1.52 eV for Re, Ir, and Pt, respectively. As shown in Table II, the bromide complexes of Re and Ir exhibited higher electronic stability than the corresponding chloride complexes whereas $PtBr_6^{2-}$ showed less electronic stability than $PtCl_6^{2-}$. We did not measure the spectra of $OsBr_6^{2-}$ because we were unable to obtain a K_2OsBr_6 salt sample. We expected that its spectra should be similar to that of $OsCl_6^{2-}$.

The vertical electron binding energies of all the measured spectral features for the seven hexahalogenometallates are summarized in Table I. The adiabatic binding energies of the *X* ground state feature, i.e., the adiabatic electron affinities of the corresponding monoanions, are given in Table II. Each species is discussed as follows.

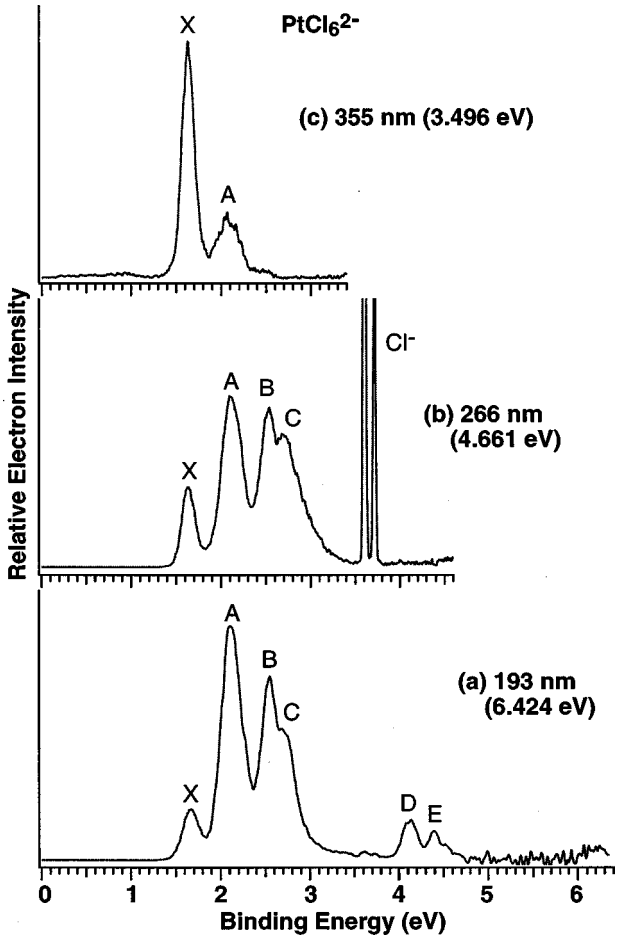

FIG. 5. Photoelectron spectra of $PtCl_6^{2-}$ at (a) 193 nm, (b) 266 nm, and (c) 355 nm.

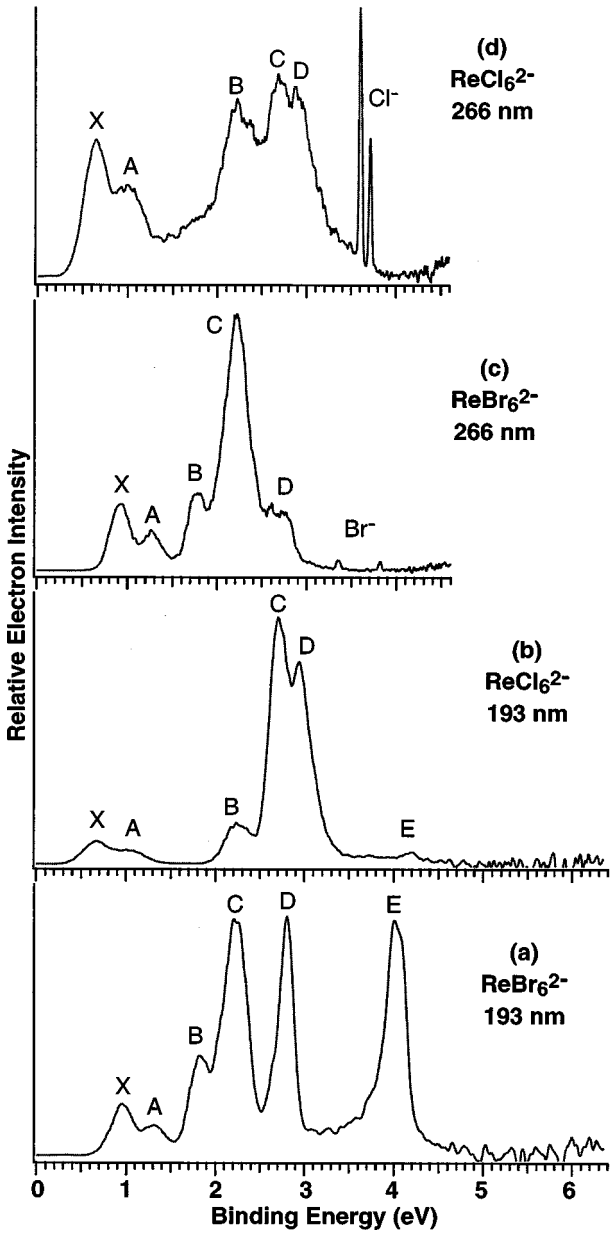

FIG. 6. Photoelectron spectra of $ReBr_6^{2-}$, compared to that of $ReCl_6^{2-}$ at 193 and 266 nm.

IV. DISCUSSION

A. Molecular orbitals and electron configurations of MCl_6^{2-} (M=Re, Os, Ir, and Pt)

The electron configurations of the central metal atoms are d^3, d^4, d^5, and d^6 in MCl_6^{2-} (M=Re, Os, Ir, Pt), respectively, where the oxidation state of the metal can be viewed as IV. Under octahedral symmetry the five d orbitals are split to a set of triply $(2t_{2g})$ and doubly $(3e_g)$ degenerate orbitals.[59] For these $5d$ transition metal hexahalogen complexes, it is known that the relatively high ligand field strength makes them inherently adopt the low-spin arrangement.[45,57] Therefore, the ground state configurations are expected to be $(2t_{2g})^3$, $(2t_{2g})^4$, $(2t_{2g})^5$, and $(2t_{2g})^6$ for MCl_6^{2-} (M=Re, Os, Ir, and Pt), respectively. The half-filled $ReCl_6^{2-}$ and the closed-shell $PtCl_6^{2-}$ complexes can maintain the O_h symmetry. However, the open shell Os and Ir complexes are expected to distort to a lower D_{4h} symmetry due to the Jahn-Teller effect.[60,61] The relatively simple spectra for the Re and Pt complexes, compared to that for the Os and Ir complexes (Fig. 1), are consistent with the higher symmetry for the former.

The chemical bonding in the hexachlorometallates have been studied theoretically.[56,57] There are significant Cl-to-M σ donations and M-to-Cl π back donations. The M–Cl bondings have considerable covalent characters. The electronic structures of MCl_6^{2-} (M=Re, Os, Ir, and Pt) were first investigated by Cotton and Harris[56] using an extended Hückel molecular orbital model, and later by Goursot *et al.*[57] using the relativistic MS-$X\alpha$ method. The highest occupied MO (HOMO) of these complexes corresponds to the $2t_{2g}$ orbital, which is mainly a nonbonding metal $5d\pi(d_{xz},d_{yz},d_{xy})$ orbital with a slight Cl $3p\pi$ contribution. The next occupied orbital $(1t_{1g})$, HOMO-1, is a nonbonding Cl $3p\pi$ orbital, according to the calculations. The next orbital $(4t_{1u})$, HOMO-2, also mainly consists of contributions from the ligand $p\pi$ orbitals with some mixing of the metal $6p$ and $4f$ orbitals. The difference among the four complexes lies at their different occupations of the HOMO$(2t_{2g})$ while the $1t_{1g}$(HOMO-1), $4t_{1u}$(HOMO-2) and other ligand-derived MOs are all completely filled. We will use these MO con-

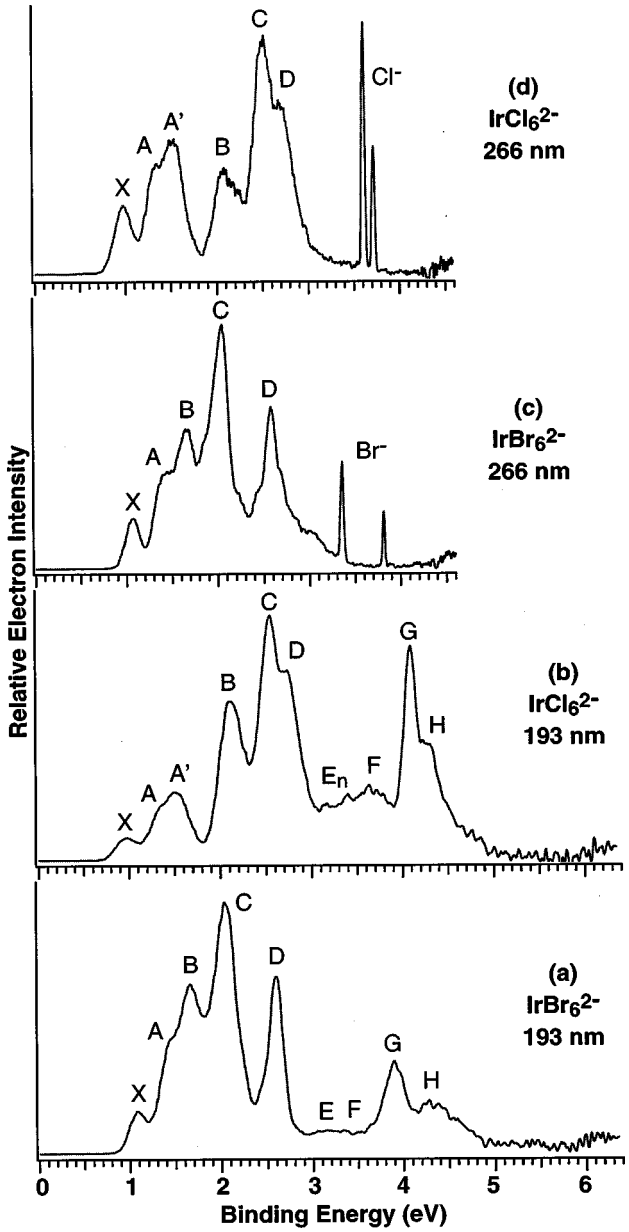

FIG. 7. Photoelectron spectra of $IrBr_6^{2-}$, compared to that of $IrCl_6^{2-}$ at 193 and 266 nm.

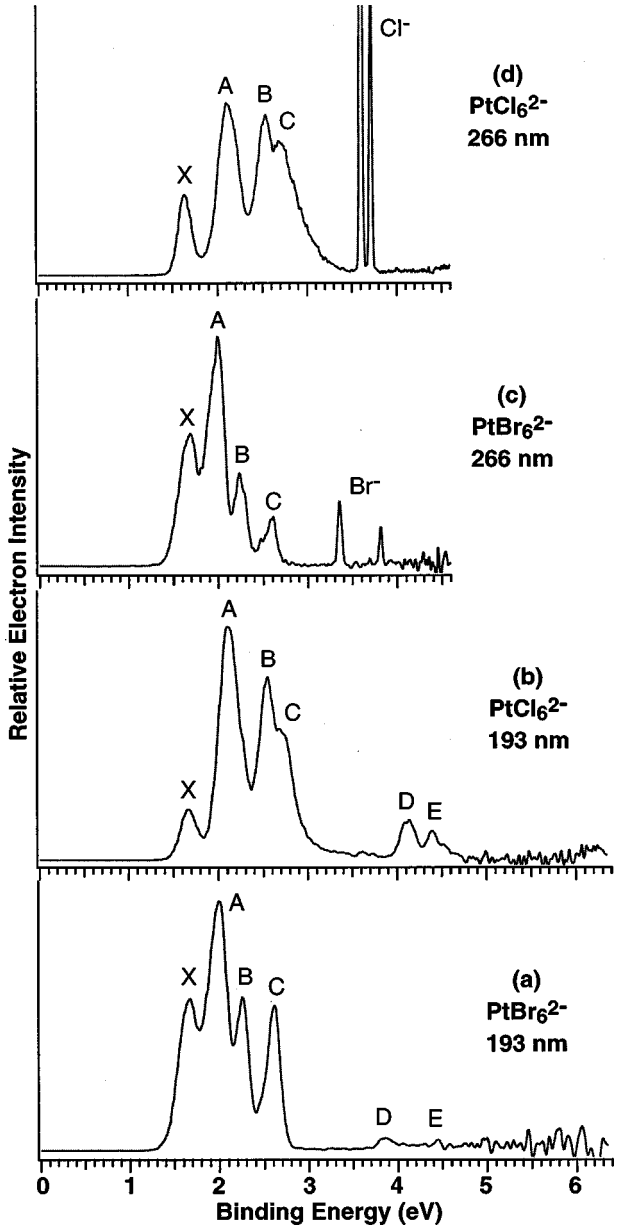

FIG. 8. Photoelectron spectra of $PtBr_6^{2-}$, compared to that of $PtCl_6^{2-}$ at 193 and 266 nm.

figurations to give a qualitative account of the major PES features observed.

B. Repulsive Coulomb barriers in MCAs and their effects on photodetachment spectra

Before discussing the PES spectra of the individual metal complexes, we first briefly explain one unique property of photodetachment of MCAs and the photon energy-dependent PES spectra. As we reported recently,[37–43] there is an essential difference between photodetachment of multiply and singly charged anions. In MCAs, there exists a RCB against electron detachment,[1,5] due to the long range Coulomb repulsion between the outgoing electron and the remaining anion (which has one less charge than the parent MCA). Figure 9 shows a schematic drawing, illustrating the RCBs bounding the MCl_6^{2-} dianion and the repulsive Coulomb potentials relative to the different asymptotic electronic states (*X*, *A*, *B*, *C*, *D*, and *E*) of the singly charged anion, MCl_6^-. The barrier height is measured from the top of a potential curve relative to an asymptotic limit of the singly charged anionic states. The well depths (energy difference between the top of the potential energy curves and the electronic ground state of the doubly charged anion) are then different for different asymptotic electronic states of the corresponding singly charged anion, as clearly shown in Fig. 9.

When a detachment photon energy is lower than the well depth of a specific singly charged anion state, but higher than its binding energy (defined as the energy difference relative to the ground state of the doubly charged anion), PES signals for this specific state and all other higher BE states cannot be observed except through electron tunnneling.[43] When the photon energy is near the top of a specific potential curve,

TABLE I. Vertical binding energies (eV)[a] of all features observed in PES spectra of MCL_6^{2-} (M=Re, Os, Ir, Pt) and MBr_6^{2-} (M=Re, Ir, Pt). All labels are referred to Figs. 1–8.

	$ReCl_6^{2-}$	$OsCl_6^{2-}$	$IrCl_6^{2-}$	$PtCl_6^{2-}$	$ReBr_6^{2-}$	$IrBr_6^{2-}$	$PtBr_6^{2-}$
X	0.67 (5)	0.64 (5)	0.98 (5)	1.67 (5)	0.96 (5)	1.09 (5)	1.67 (5)
A	1.04 (10)	1.41 (5)	1.35 (5)	2.12 (5)	1.32 (5)	1.45 (8)	1.99 (5)
			1.52 (5) (A)				
B	2.25 (10)	2.12 (5)	2.12 (5)	2.55 (5)	1.83 (5)	1.67 (5)	2.25 (5)
C	2.70 (5)	2.61 (5)	2.55 (5)	2.72 (5)	2.23 (5)	2.05 (5)	2.61 (5)
D	2.94 (5)	2.82 (5)	2.72 (5)	4.12 (5)	2.80 (5)	2.60 (5)	3.85 (5)
E	4.21 (10)	3.23 (5) (E_1)	3.17 (5) (E_1)	4.40 (10)	4.02 (5)	~3.2	4.45 (10)
		3.35 (5) (E_2)	3.40 (5) (E_2)				
F		3.52 (5) (F_1)	3.64 (5)			~3.4	
		3.60 (5) (F_2)					
		3.87 (5) (F_3)					
G		4.11 (10)	4.10 (5)			3.90 (5)	
H			4.29 (10)			4.33(10)	

[a]The numbers in the parentheses indicate the uncertainties in the last digits.

the detached electron signal corresponding to this state will be reduced. The relevant parameters and states used in Fig. 9 are actually for that of $PtCl_6^{2-}$, which we use as an example here.

Figure 5 shows the PES spectra of $PtCl_6^{2-}$ at 193, 266, and 355 nm. Six distinct features were resolved in the 193 nm spectrum, labeled as *X*, *A*, *B*, *C*, *D*, and *E*. The latter two features (*D* and *E*) completely disappeared in the 266 nm spectrum [Fig. 5(b), the two sharp peaks were due to Cl^-]. In the 355 nm spectrum [Fig. 5(c)], the B and C features disappeared while the intensity of the A feature was significantly reduced. In fact, we have tried to measure the spectrum of $PtCl_6^{2-}$ at 532 nm (2.331 eV, higher than the *X* state binding energy), but no electron signals could be detected. These observations of the photon energy dependence can be easily understood using the schematic potential energy curves, shown in Fig. 9, where the positions of the four photon energies used and the vertical BEs of the six observed states are shown. The 193 nm photon was near the barrier top of the *E* and *D* state; the weak intensities of these two states were likely due to the barrier effect. There may very well be other states between 4.5 and 6.4 eV, which would not be observed at 193 nm. The 266 nm photon was above the barrier tops of the *X*, *A*, *B*, and *C* states, but below that of the *D* and *E* states. The 355 nm photon should be above the barrier top of the *X* state, but below that of the *A* state. Thus the weaker signal of the *A* state in the 355 spectrum must be due to electron tunneling. Finally, the 532 nm photon was below the barrier top of the *X* state and no electron signals were expected to be observed.

If we assume that the RCBs all have the same height for the different electronic states (in reality they may be slightly different depending on which electron is removed), we can estimate the RCB height from the photon-energy-dependent PES spectra. Since the 193 nm (6.424 eV) photon was near the barrier top of the *E* state which has a vertical BE of about 4.40 eV, we obtained that the RCB should be about 2 eV (6.424 eV−4.40 eV). Since the 355 nm (3.496 eV) photon was below the *A* state (vertical BE, 2.12 eV), we could infer that the RCB was larger than 1.4 eV (3.496 eV−2.12 eV), consistent with the estimate from the 193 nm spectrum above. As shown in Fig. 9, the 266 nm photon was near the barrier top of the *C* state, which became slightly more intense and broader at 266 nm compared to that at the 193 nm. As will be discussed below, these observations for the *C* state were really due to an autodetachment effect at 266 nm. Otherwise, a significantly reduced intensity should be observed at 266 nm for the *C* state due to the barrier effect. A brief glance of the 193 nm spectra of all the four dianions (Fig. 1) revealed that there were no higher BE features for all four complexes beyond about 4.5 eV, due to the RCB. We will address the issue of the RCB separately for each species below when discussing the photon energy-dependent PES.

TABLE II. Measured adiabatic electron binding energies (ADE, eV) and estimated repulsive coulomb barriers (RCB, eV) of the seven ML_6^{2-} complexes along with their redox potentials (E_{rd},*V*) in solution and the calculated adiabatic electron affinities (EA, eV) of ML_6^-.

	$ReCl_6^{2-}$	$OsCl_6^{2-}$	$IrCl_6^{2-}$	$PtCl_6^{2-}$	$ReBr_6^{2-}$	$IrBr_6^{2-}$	$PtBr_6^{2-}$
ADE[a]	0.46(5)	0.46(5)	0.82(5)	1.58(5)	0.76(6)	0.96(6)	1.52(6)
EA[b]	0.26	−0.23	0.53	1.28			
E_{rd}^b	1.33	1.28	1.74	2.30			
RCB	~2.4	~2.0	~1.7	~2.0	~2	⩽2	~2.5

[a]The ADE of ML_6^{2-} is the same as the adiabatic EA of ML_6^-. The numbers in the parentheses indicate the uncertainties in the last digt.
[b]From Ref. 51.

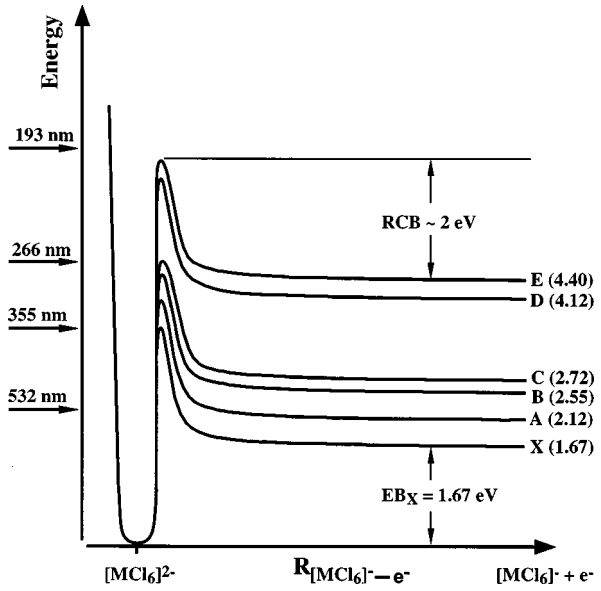

FIG. 9. Schematic drawing of potential energy curves showing the repulsive Coulomb barriers (RCB) of a dianion with respect to different final states (*X* to *E*) of the corresponding singly charged anion. The binding energies in eV and the estimated RCB for $PtCl_6^{2-}$ are shown (see text). The relative positions of the four photon energies used are also indicated.

C. $PtCl_6^{2-}$ and $PtBr_6^{2-}$

We first discuss the PES spectra of $PtCl_6^{2-}$ and $PtBr_6^{2-}$, which both have closed shell MO configurations. The photon energy dependent PES spectra of $PtCl_6^{2-}$ (Fig. 5) have already been briefly mentioned above. The two sharp peaks at 3.61 and 3.71 eV in the 266 nm spectrum [Fig. 5(b)] are due to Cl^- as a result of photodissociation ($PtCl_6^{2-}+h\nu \rightarrow PtCl_5^-+Cl^-$) and subsequent photodetachment of Cl^-($Cl^-+h\nu \rightarrow Cl+e^-$) at 266 nm. This two-photon process was confirmed by photon-flux-dependent studies. In fact, very weak signals due to Cl^- were also discernible in the 193 nm spectrum [Figs. 1(d) and 5(a)]. The second fragmentation product ($PtCl_5^-$) was expected to have much higher electron binding energies and could probably not be detached at 266 nm. As mentioned above, the intense and broad *C* feature at 266 nm [Fig. 5(b)] was likely due to autodetachment,[62] i.e., the $PtCl_6^{2-}$ dianion resonantly absorbed a 266 nm photon to form a temporary excited state, which then decayed to the *C* state. Both the enhanced intensity and the broad nature of this feature at 266 nm were consistent with the autodetachment mechanism.

The spectra of $PtBr_6^{2-}$ are compared to that of $PtCl_6^{2-}$ in Fig. 8 at 266 and 193 nm. The $PtBr_6^{2-}$ complex gave nearly identical spectra as $PtCl_6^{2-}$. At 266 nm, even the Br^- signals [Fig. 8(c)] due to photodissociation of the parent dianions were similar to the Cl^- signals in the $PtCl_6^{2-}$ spectrum [Fig. 8(d)]. From the photon energy-dependent spectra of $PtBr_6^{2-}$, however, we inferred a larger RCB for $PtBr_6^{2-}$ than that for $PtCl_6^{2-}$. The very weak intensity of the *D* feature (vertical BE, 3.85 eV) in the $PtBr_6^{2-}$ spectrum [Fig. 8(a)] indicated that the 193 nm photon was probably below the RCB of the *D* state, giving a barrier height of ~2.5 eV or larger (6.424 eV–3.85 eV). The reduced intensities of the *B* and *C* features in the 266 spectrum of $PtBr_6^{2-}$ [Fig. 8(c)] were consistent with this large RCB. The higher RCB in the bromide complex suggests that there is a larger Coulomb repulsion in $PtBr_6^{2-}$ than that in $PtCl_6^{2-}$. The slightly smaller adiabatic electron binding energy of $PtBr_6^{2-}$ (Table II) is consistent with this observation.

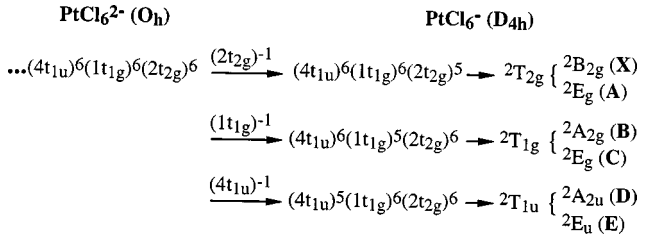

FIG. 10. Schematic diagram showing various one-electron detachment channels for $PtCl_6^{2-}$. Letters in the parentheses represent a tentative assignment of the detachment features of $PtCl_6^{2-}$ [see Figs. 1(d) and 5].

As discussed above, the ground state of $PtCl_6^{2-}$ adopts an electron configuration of $\ldots(4t_{1u})^6(t1_{1g})^6(2t_{2g})^6$, which is closed shell and will be stable under O_h symmetry. Figure 10 shows the one-electron detachment channels expected from this configuration; the final states of $PtCl_6^-$ are $^2T_{2g}$, $^2T_{1g}$, and $^2T_{1u}$, upon detaching one electron from the $2t_{2g}$, $1t_{1g}$, and $4t_{1u}$, respectively. All these degenerate states are expected to be unstable under the O_h symmetry due to the Jahn-Teller effect and are expected to distort to the lower D_{4h} symmetry.[60,61] Under D_{4h} symmetry, each of the three electronic states will split to two terms, yielding totally six electronic states, as shown in Fig. 10. We tentatively assign the six features (*X*, *A*, *B*, *C*, *D*, and *E*) observed in the PES spectra [Figs. 1(d) and 5] to these six electronic states, as given in Fig. 10. All the *E* states are still doubly degenerate and could further split with a further decrease of symmetry. However, such splittings, if taking place, were not resolved in the PES spectra.

These assignments are supported by the PES spectra of $PtBr_6^{2-}$. Figure 8 shows the PES of $PtBr_6^{2-}$ at 193 and 266 nm along with the $PtCl_6^{2-}$ spectra for comparison. There are also six features (labeled *X* to *E*) in the 193 nm spectra of $PtBr_6^{2-}$. The *X* and *A* features and their separation are very similar to that in the $PtCl_6^{2-}$ spectra, except that the peaks slightly shift to lower BE by ~0.1 eV in $PtBr_6^{2-}$. It is thus reasonable to assign the *X* and *A* features to be due to detachment from the metal *d*-orbitals in both the chloride and bromide complexes. There are also two pairs of features *B*/*C* and *D*/*E* in the $PtBr_6^{2-}$ spectra, similar to that in the $PtCl_6^{2-}$ spectra, but with much larger separations in the bromide case. The large separations of these features in $PtBr_6^{2-}$ provide rather solid evidence that they are due to detachment from ligand-based orbitals, as a result of the anticipated stronger vibronic coupling in the bromide complex.[61] However, we also noted that the *B*/*C* splitting in the spectra of $PtCl_6^{2-}$ and $PtBr_6^{2-}$ seemed to correlate with the spin–orbit splittings of Cl and Br, as clearly shown from the Cl^- and Br^- PES features in the 266 nm spectra. This was perhaps not surprising, considering the nonbonding and predominantly ligand-nature of the $1t_{1g}$ MO.

D. $ReCl_6^{2-}$ and $ReBr_6^{2-}$

The PES spectra of $ReCl_6^{2-}$ at 193, 266, 355, and 532 nm are shown in Fig. 2. There are six well-resolved spectral features (labeled as *X, A, B, C, D*, and *E*) in the 193 nm spectrum. The *E* feature was very weak at 193 nm [Fig. 2(a)], suggesting that the 193 nm photon was probably below the RCB of the *E* state. The sharp Cl^- peaks in the 266 nm spectrum [Fig. 2(b)] were due to photodissociation of the parent $ReCl_6^{2-}$ dianion and subsequent photodetachment of the free Cl^-, similar to the $PtCl_6^{2-}$ case [Fig. 5(b)]. From the weak *E* feature (vertical BE, 4.21 eV) at 193 nm, we inferred that the RCB height should be >2.2 eV (6.242 eV−4.21 eV). The 266 nm photon was then expected to be below the RCB of the *C* and *D* states, which have vertical BEs of 2.70 and 2.94 eV (Table I), respectively. Their reduced intensities at 266 nm were consistent with the above estimated RCB. There seemed to be a broad background from about 1.5 to 3.5 eV in the 266 nm spectrum of $ReCl_6^{2-}$ [Fig. 2(b)], possibly due to either autodetachment or photodetachment of other low BE singly charged $ReCl_x^-$ species due to photodissociation. At 355 nm [Fig. 2(c)], all the higher BE features (*B, C*, and *D*) disappeared due to the RCB. The reduced relative intensity of the *A* feature at 355 nm suggested that the 355 nm photon was near the barrier top of the *A* state (vertical BE, 1.04 eV), yielding a RCB height of ~2.4 eV (3.496 eV−1.04 eV), consistent with the estimate using the *E* feature at 193 nm [Fig. 2(a)]. The 532 nm photon was expected to be near the RCB of the *X* state, which was the only feature observed at 532 nm [Fig. 2(d)].

The PES spectra of $ReBr_6^{2-}$ at 193 and 266 nm are compared to that of $ReCl_6^{2-}$ in Fig. 6. All the features in $ReBr_6^{2-}$ can be correlated to those in $ReCl_6^{2-}$ according to the same labels as indicated in Fig. 6, except that the binding energies of the *X* and *A* features increased in $ReBr_6^{2-}$ while the binding energies of the other features (*B* to *E*) decreased. In particular, the intensity of the *E* feature in $ReBr_6^{2-}$ was significantly enhanced, suggesting that the 193 nm photon was above the RCB of the *E* state (vertical BE, 4.02 eV). Thus the RCB height of $ReBr_6^{2-}$ should be <2.4 eV (6.424 eV−4.02 eV). The *E* feature completely disappeared in the 266 nm spectrum [Fig. 6(c)], where two sharp peaks due to Br^- were visible. The intensity of the *D* feature was significantly reduced at 266 nm, indicating that the 266 nm photon was below the RCB of the *D* state (vertical BE, 2.80 eV). Therefore, the RCB should be >1.86 eV (4.661 eV−2.80 eV). The intensity of the *C* feature (vertical BE, 2.23 eV) did not change significantly at 266 nm, suggesting that that RCB should be <2.4 eV, consistent with the estimate from the 193 nm above based on the *E* sate. Therefore, we estimated a RCB of ~2 eV for $ReBr_6^{2-}$ (1.86 eV<RCB<2.4 eV).

The ground state of $ReCl_6^{2-}$ has an electron configuration of $\ldots(4t_{1u})^6(t1_{1g})^6(2t_{2g})^3$ with a half-filled HOMO ($2t_{2g}$), which is expected to be stable under O_h symmetry without first order Jahn-Teller distortions. Figure 11 shows the first few one-electron detachment channels, based on this configuration. Detaching one electron from $2t_{2g}$, $1t_{1g}$, and $4t_{1u}$ leads to the following final states of $ReCl_6^-$, $^3T_{1g}$, $^5T_{2g}$, and $^5T_{2u}$, respectively. Triplet states can also be formed upon removing an electron from $1t_{1g}$ or $4t_{1u}$, but are not shown in Fig. 11 because they were expected to have higher energies. All these final states are degenerate and expected to undergo Jahn-Teller distortion to a lower D_{4h} symmetry, as given in Fig. 11. The first three low BE features (*X, A* and *B*) in the $ReCl_6^{2-}$ spectra (Fig. 2) have relatively low intensity and their intensity ratios were invariant at 266 nm [Fig. 2(b)]. We assigned these three features to be derived from detachment of a *d*-electron from the $2t_{2g}$ HOMO. The three features were attributed to the Jahn-Teller splittings of the $^3T_{1g}$ state, as given in Fig. 11. The *C* and *D* pair was assigned to be due to removal of an electron from the ligand orbital, $1t_{1g}$. Even though the *E* feature has very low intensity [Fig. 2(a)], it was real. Its feeble intensity was due to the RCB. Comparing to other complexes (Fig. 1), we expected that there should also be a pair of state associated with the *E* state. The other component was not observed at 193 nm due to the RCB. We thus assigned the *E* feature of $ReCl_6^{2-}$ [Figs. 1(a) and 2(a)] to be due to removal of an electron from the $4t_{1u}$ ligand MO, as shown in Fig. 11. We see from Fig. 11 that we attributed the *X* and *A* features in the spectra of $ReCl_6^{2-}$ [Figs. 1(a) and 6] to be due to the further Jahn-Teller splitting of the ^3E_g state. However, the *D* and *E* features (Fig. 6), which were attributed to the ^5E_g and ^5E_u states, respectively, did not show any resolved splittings. Clearly, a detailed assignment was not possible without further accurate *ab initio* calculations. The current discussion should be viewed as tentative.

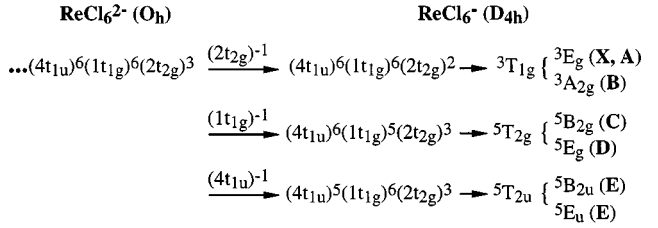

FIG. 11. Schematic diagram showing various one-electron detachment channels for $ReCl_6^{2-}$. Letters in the parentheses represent a tentative assignment of the detachment features of $ReCl_6^{2-}$ [see Figs. 1(a) and 2].

Nevertheless, as shown in Fig. 6, the PES spectra of $ReBr_6^{2-}$ support the above spectral assignments for $ReCl_6^{2-}$ in terms of the origins of the different features. The fact that the *X, A*, and *B* features (Fig. 6) have relative small intensities and similar patterns in both complexes indicates that they are due to detaching a metal $5d$ electron. The large separation of the *C* and *D* features in $ReBr_6^{2-}$ indicates clearly that they are due to removing one electron from the ligand orbitals. The observation of the strong *E* feature in the $ReBr_6^{2-}$ spectrum confirmed the *E* feature in the $ReCl_6^{2-}$ spectrum. As discussed above, the strong *E* feature in $ReBr_6^{2-}$ was due to the smaller RCB (~2 eV) in $ReBr_6^{2-}$, in comparison to the RCB (~2.4 eV) in $ReCl_6^{2-}$. The smaller RCB in $ReBr_6^{2-}$ is consistent with a slightly higher electronic stability of the bromide complex, suggesting that there is a slightly smaller Coulomb repulsion in the $ReBr_6^{2-}$ dianion.

E. $OsCl_6^{2-}$

Figure 3 shows the PES spectra of $OsCl_6^{2-}$ at four detachment photon energies. Compared to the spectra of $PtCl_6^{2-}$ and $ReCl_6^{2-}$, the spectra of $OsCl_6^{2-}$ were more complicated. In particular, extra features appeared in the spectrum of $OsCl_6^{2-}$ between 3 and 4 eV, labeled as E_n and F_n, which did not exist in the spectra of $PtCl_6^{2-}$ and $ReCl_6^{2-}$ (Fig. 1). There seemed to be fine structures in each of the E_n and F_n bands, which are listed in Table I as E_n $(n=1,2)$ and F_n $(n=1-3)$, respectively. Again, at 266 nm, the higher BE features disappeared due to the RCB. The sharp peaks of Cl^- due to photodissociation were also visible. The feature *D* (vertical BE, 2.82 eV) was almost cutoff at 266 nm [Fig. 3(b)], i.e., the 266 nm photon was likely below the RCB of the *D* state. Thus, we estimated that the RCB in $OsCl_6^{2-}$ should be >1.8 eV (4.661 eV−2.82 eV). Since the intensity of the *C* feature (vertical BE, 2.61 eV) was also reduced at 266 nm, we surmised that the 266 nm photon was probably near the barrier top of the *C* state. We thus inferred that the RCB in $OsCl_6^{2-}$ should be ~2 eV. More high BE features were missing in the 355 nm spectrum [Fig. 3(c)], as expected. The 355 nm photon was expected to be near or above the RCB of the *A* feature, which should be observed at 355 nm. However, its much broader width at 355 nm [Fig. 3(c)] was surprising. We again attributed this to an autodetachment process, similar to those observed in $PtCl_6^{2-}$ at 266 nm, as discussed above. The 532 nm photon should be near the barrier top of the *X* state, which was indeed the only feature observed.

Under O_h symmetry, $OsCl_6^{2-}$ is expected to have a configuration of $\ldots(4t_{1u})^6(1t_{1g})^6(2t_{2g})^4$, which, unlike $PtCl_6^{2-}$ and $ReCl_6^{2-}$, is expected to undergo Jahn-Teller distortion to a lower D_{4h} symmetry.[60,61] The more complicated PES spectra of $OsCl_6^{2-}$ might be related to the initial state Jahn-Teller effect. We will only give a very qualitative account of the spectral features, by comparing with the other MCl_6^{2-} complexes. The first three low BE features (*X*, *A*, and *B*) were similar to those in $ReCl_6^{2-}$ (Fig. 1) and should be due to removal of electrons from *d*-orbitals $(2t_{2g})$. The *C* and *D* features in $OsCl_6^{2-}$ were similar to the same *C*/*D* pair of features in $ReCl_6^{2-}$ and the *B*/*C* features in $PtCl_6^{2-}$ (Fig. 1), and should be due to detachment from the similar ligand-dominated MO, $1t_{1g}$. The feature *G* in $OsCl_6^{2-}$ was similar to the feature *E* in $ReCl_6^{2-}$ and feature *D* in $PtCl_6^{2-}$ (Fig. 1) and was attributed to detachment from the $4t_{1u}$MO. The extra features, E_n and F_n were probably due to the initial state Jahn-Teller splittings and could not be assigned currently without knowledge about the precise electron configurations of $OsCl_6^{2-}$. The lack of comparable data on $OsBr_6^{2-}$ also made it difficult to corroborate any more definitive assignments.

F. $IrCl_6^{2-}$ and $IrBr_6^{2-}$

Figure 4 shows the PES spectra of $IrCl_6^{2-}$ at four photon energies. The spectra of $IrCl_6^{2-}$ exhibited remarkable similarities to that of $OsCl_6^{2-}$, as shown in Fig. 1 at 193 nm, except that the feature around 1.5 eV seemed to be a doublet (*A* and *A*′) in $IrCl_6^{2-}$. The 266 nm spectrum of $IrCl_6^{2-}$ again showed the Cl^- peaks due to photodissociation and the anticipated disappearance of the high BE features due to the RCB. The relative intensity of the feature *D* (vertical BE, 2.72 eV) did not change at 266 nm suggesting that the 266 nm photon was above the RCB to the *D* state. We thus estimated a RCB of <1.9 eV(4.661 eV−2.72 eV). At 355 nm, more high BE features disappeared. Clearly, the 355 nm photon was below the RCB to the *B* state (vertical BE, 2.12 eV), suggesting that the RCB should be >~1.4 eV(3.496 eV −2.12 eV). The RCB thus appeared to be somewhat lower in $IrCl_6^{2-}$ (~1.7 eV, averaging over the upper and lower bounds). This was already indicated by the rather strong *G* and *H* features in the 193 nm spectrum of $IrCl_6^{2-}$, compared to the weak high BE features in the 193 nm spectra of the other complexes (Fig. 1). The 532 nm photon was below the RCB to the *X* state, and the signals observed in the 532 nm spectrum were due to electron tunneling, consistent with the weak intensity of the 532 nm spectrum [Fig. 4(b)]. The total count rates of the 532 nm spectrum were very low and rather high detachment-laser-photon fluxes had to be used.

The 193 and 266 nm spectra of $IrBr_6^{2-}$ are compared with those of $IrCl_6^{2-}$ in Fig. 7. Similar spectral features were observed for $IrBr_6^{2-}$ as for $IrCl_6^{2-}$. Analogous to other MBr_6^{2-} complexes, the higher BE features (*B* to *H*) all shifted to lower BEs even though the BEs of the *X* and *A* features were increased [Fig. 7(a)]. Thus, the spacing between the *A* and *B* features was significantly reduced in the $IrBr_6^{2-}$ spectrum, where the doublet (*A* and *A*′) that appeared in $IrCl_6^{2-}$ [Fig. 7(b)] could no longer be resolved. The spacings between the *C* and *D* features, and between the *G* and *H* features were increased, as observed in the other MBr_6^{2-} complexes. Similar spectral features between *D* and *G* were discernible in the $IrBr_6^{2-}$ spectrum (*E* and *F*), but appeared to be much weaker than those in $IrCl_6^{2-}$. At 266 nm, sharp features due to Br were observed and the high BE features again disappeared due to the RCB. The intensity of the *D* feature (vertical BE, 2.60 eV) did not seem to vary at 266 nm, suggesting that the RCB in $IrBr_6^{2-}$ should be ⩽2 eV(4.661 eV−2.60 eV).

Under O_h symmetry, $IrCl_6^{2-}$ has a configuration of $\ldots(4t_{1u})^6(1t_{1g})^6(2t_{2g})^5$, which is expected to undergo Jahn-Teller distortions to a lower D_{4h} symmetry, similar to $OsCl_6^{2-}$. We will again only give a very qualitative account of the spectral features, by comparing with the other MCl_6^{2-} complex, in particular to that of $OsCl_6^{2-}$. The first four low BE features (*X*, *A*, *A*′, and *B*) are similar to the low BE features (*X*, *A*, and *B*) in both $OsCl_6^{2-}$ and $ReCl_6^{2-}$ (Fig. 1), except that the intensity of the *B* feature in $IrCl_6^{2-}$ appeared to be stronger. We thus attributed these lower BE features to be due to removal of electrons from *d*-orbitals $(2t_{2g})$, as indicated in Fig. 1. The *C* and *D* features in $IrCl_6^{2-}$ appeared in all the four complexes (Fig. 1) and should be due to detachment from the similar ligand-dominated MO, $1t_{1g}$. The features *G* and *H* in $IrCl_6^{2-}$ also have counterparts in the other four complexes and were attributed to detachment from the $4t_{1u}$MO. The extra features (E_n and *F*) in $IrCl_6^{2-}$ were similar to those in $OsCl_6^{2-}$, and again probably due to the initial state Jahn-Teller splittings. The qualitative assignments of the $IrCl_6^{2-}$ spectra were supported by the spectra of

$IrBr_6^{2-}$. The anticipated enhanced splittings between the *C* and *D* features, and *G* and *H* features were indeed observed, consistent with the assignments that they were due to the ligand-based MOs.

G. Overview

The current experiments represent the first observation of these hexahalogenometallate dianions in the gas phase. All of these species exhibit positive electron binding energies, indicating they are electronically stable. They are also likely to be stable thermodynamically although our experiments did not provide direct information about the thermodynamic stability. Because there also exists a potential barrier against dissociation of the type, $ML_6^{2-} \rightarrow ML_5^- + L^-$, these complexes could be just locally stable. They are at least long-lived in the gas phase, considering our experimental time scale ($\sim$0.1 s).

The PES data provide unprecedented detailed molecular electronic structure information about the hexahalogenometallates in the gas phase, even though only very qualitative discussions were given here. The obtained spectroscopic information should be valuable to compare to more accurate theoretical investigations. Despite of the qualitative nature of the current assignments, features due to *d*-orbitals or ligand-orbitals could be clearly distinguished, as indicated in Fig. 1. As discussed above, these assignments were corroborated by similar results on the bromide complexes. It is interesting that detachment of *d*-electrons all happened at lower binding energies than those from the ligands. It is also important to point out that the spectra shown in Figs. 1–8 all represent electronic states of the ML_6^- singly charged anions. The feature *X* represents the ground state of the monoanions in each case whereas all the other features represent the excited electronic states of the monoanions. The spacings of the excited state features relative to the *X* ground state correspond to the excitation energies. All the higher BE features due to the *d*-electrons can be related to low energy $d-d$ transitions whereas all the features due to the ligands can be related to $L \rightarrow M$ charge transfer transitions within the monoanions. The excitation energies for these transitions can be estimated from the vertical binding energies given in Table I.

The repulsive Coulomb barrier is a fundamental property of any MCAs. As we have shown previously, the heights of the RCB in MCAs are equivalent to the Coulomb repulsion energies among the excess charges at the equilibrium MCA geometry. The estimated RCBs for the seven complex dianions are given in Table II. It is noteworthy that $ReCl_6^{2-}$ and $PtBr_6^{2-}$ seemed to have larger RCBs than the other complexes, whereas $IrCl_6^{2-}$ appeared to have a rather low RCB. Because of the covalent character between the M–Cl bonds in these complexes, we cannot simply view them as an M^{4+} ion interacting with $6Cl^-$. Therefore, the Coulomb repulsion energies in these dianions might be an important parameter in future theoretical understanding of the structure and bonding of these metal complexes. It would be interesting to investigate if the RCB is the same for the different asymptotic states of the monoanion. As mentioned above, the RCB represents the intramolecular Coulomb repulsion energies within the dianions. It would be interesting to investigate theoretically if the RCB correlates with the M–L bond lengths, i.e., the sizes of the dianions. In particular, the larger RCB in $PtBr_6^{2-}$ and its decreased electronic stability in comparison to $PtCl_6^{2-}$ is unusual and may suggest subtle chemical bonding changes in the two dianions.

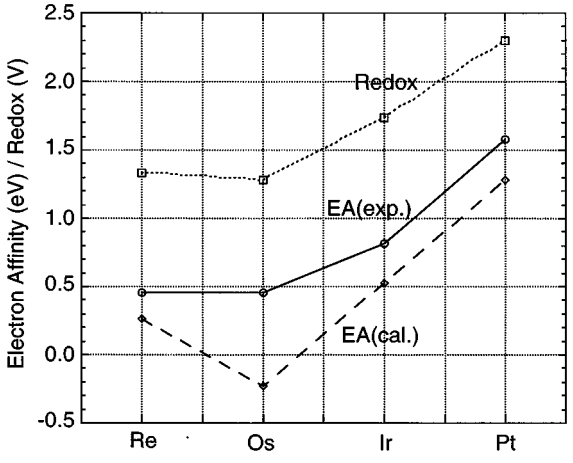

FIG. 12. Correlation between our measured [EA(expt)] and calculated [EA(cale), Ref. 51] adiabatic electron affinities of MCl_6^- (M=Re, Os, Ir, and Pt) and the redox potentials of the corresponding dianions, MCl_6^{2-}, in solution (Ref. 51).

H. Electron affinities and redox potentials

The adiabatic electron affinities (EAs) of the singly charged anions, measured from the thresholds of the PES spectra of the corresponding dianions, indicate the electronic stability of the doubly charged anions. The EAs of the seven complex monoanions are given in Table II. For the four chloride anions, there has been a recent calculation by Macgregor and Moock.[51] Table II shows that their calculated EAs are consistent with our measured values and show the same trend (also see Fig. 12), although the calculations in general underestimated the EAs. In particular, the calculations gave a negative EA for $OsCl_6^{2-}$, i.e., the calculation predicted that the $OsCl_6^{2-}$ dianion was not electronically stable, in contrast to the current experimental observation. Since the classic work of Bartlett and co-workers,[63] the EAs of neutral hexafluorides of the third transition series have attracted considerable attention and they are generally believed to increase in the direction, $WF_6 < ReF_6 < OsF_6 < IrF_6 < PtF_6$. The available experimental data on the gas phase EAs of the neutral hexafluorides have been interpreted as confirming Bartlett's general conclusion of this EA trend across a transition metal row, due to the inefficient shielding of the core charges of the metal by the *d*-electrons. Our measured EAs of the ML_6^- monoanions also seem to be consistent with this trend. Within our experimental accuracy, however, the EAs of $ReCl_6^-$ and $OsCl_6^-$ are the same, whereas the calculations predicted a decrease from the Re to Os complex. The latter has been interpreted as arising from effects of interelectronic correlation and repulsion in the theoretical study.[51]

An oxidation reaction is a one-electron process and proceeds according to $[MX_6]^{2-} \rightarrow [MX_6]^- + e^-$, which, beside

the solvation effects, is similar to electron detachment in the gas phase. Therefore, the gas phase EAs should be inherently related to the redox potentials, except that the solvation effects essential in redox processes in solution are missing in the electron detachment in vacuum. In Table II and Fig. 12, the redox potentials for MCl_6^{2-} (M=Re, OS, Ir, and Pt) from the literature[51] are compared with our measured EAs. It is seen clearly that there is a remarkable correlation between our measured EAs for the hexachloride complexes and their redox potentials, suggesting that the solvation energies for all the relevant ions are probably similar in these cases. This is perhaps not surprising because the size of these anions, i.e., the M–Cl bond distances, are indeed very similar in the condensed phases.[51]

V. CONCLUSIONS

We have observed for the first time several hexahalogenometallates dianions, ML_6^{2-} (M=Re, Os, Ir, and Pt; L=Cl and Br) in the gas phase. These free dianions were found to be stable electronically with positive electron binding energies. The photodetachment photoelectron spectra of these metal complex dianions provided a wealth of electronic structure information of both the dianions and the singly charged anions. Detachment features from the metal *d*-orbitals and ligand-based orbitals were observed and could be distinguished. All the features due to the metal *d*-orbitals occurred at low binding energies whereas those due to the ligands all had rather high binding energies. The photodetachment features were qualitatively interpreted based on the molecular orbital configurations under O_h symmetry. Definite assignments would require accurate theoretical calculations. The photoelectron spectra of the Re and Pt complexes appeared to be slightly simpler than those from the Os and Ir complexes, consistent with the fact that the latter have degenerate electronic states in the dianion ground states and are subjective to Jahn-Teller distortions. The bromide complexes gave similar spectral features as those from the chloride and allowed features from the ligands to be more clearly distinguished. The second excess electron in $ReBr_6^{2-}$ and $IrBr_6^{2-}$ were observed to be stabilized more than that in the corresponding chloride dianions whereas the opposite was observed in the Pt complexes.

Photon energy-dependent studies clearly revealed the effects of the repulsive Coulomb barriers, which are important in understanding free multiply charged anions. The barrier heights were estimated from the photon-energy-dependent spectra. The barrier heights, which are equivalent to the net Coulomb repulsion energies in the dianions, are all around 2 eV, except for $ReCl_6^{2-}$ and $PtBr_6^{2-}$, which have slightly higher barrier heights, ~2.4 and ~2.5 eV, respectively, and $IrCl_6^{2-}$, appeared to have a particularly low RCB (~1.7 eV). The first few low binding energy features (between 0.5–2.2 eV) in each PES spectrum are due to removal of a *d*-electron from the transition metal, corresponding to an oxidation reaction [M(IV)→M(V)] *in vacuo*. Indeed we found that the adiabatic electron binding energies measured in the gas phase for the metal complex dianions have a close correlation with their corresponding redox potentials measured in solutions.

ACKNOWLEDGMENTS

We thank Dr. M. Gutowski for valuable discussions. This work was supported by the U.S. Department of Energy Office of Basic Energy Sciences, Chemical Science Division. Acknowledgment is also made to the Donors of the Petroleum Research Fund, administered by the American Chemical Society, for partial support of this research. This work was performed at the W. R. Wiley Environmental Molecular Sciences Laboratory, a national scientific user facility sponsored by Department of Energy's Office of Biological and Environmental Research and located at Pacific Northwest National Laboratory. Pacific Northwest National laboratory is operated for the U.S. Department of Energy by Battelle under Contract No. DE-AC06-76RLO 1830. L. S. W. is an Alfred P. Sloan Foundation Research Fellow.

[1] M. K. Scheller, R. N. Compton, and L. S. Cederbaum, Science **270**, 116 (1995).
[2] J. Kalcher and A. F. Sax, Chem. Rev. **94**, 2291 (1994).
[3] A. I. Boldyrev, M. Gutowski, and J. Simons, Acc. Chem. Res. **29**, 497 (1996).
[4] G. R. Freeman and N. H. March, J. Phys. Chem. **100**, 4331 (1996).
[5] R. N. Compton, *Negative Ion States*, in *Photophysics and Photochemistry in the Vacuum Ultraviolet*, edited by S. P. McGlynn (Reidal, the Netherlands, 1985).
[6] A. Adamowicz, J. Chem. Phys. **95**, 8669 (1991).
[7] J. D. Watts and R. J. Bartlett, J. Chem. Phys. **97**, 3445 (1992).
[8] M. K. Scheller and L. S. Cederbaum, J. Phys. B **25**, 2257 (1992).
[9] T. Sommerfeld, M. K. Scheller, and L. S. Cederbaum, Chem. Phys. Lett. **209**, 216 (1993).
[10] A. I. Boldyrev and J. Simons, J. Chem. Phys. **98**, 4745 (1993).
[11] H.-G. Weikert and L. S. Cederbaum, J. Chem. Phys. **99**, 8877 (1993).
[12] M. K. Scheller and L. S. Cederbaum, Chem. Phys. Lett. **216**, 141 (1993).
[13] M. K. Scheller and L. S. Cederbaum, J. Chem. Phys. **99**, 441 (1993).
[14] A. I. Boldyrev and J. Simons, J. Phys. Chem. **98**, 2298 (1994).
[15] M. K. Scheller and L. S. Cederbaum, J. Chem. Phys. **101**, 3962 (1994).
[16] M. K. Scheller and L. S. Cederbaum, J. Chem. Phys. **100**, 8934 (1994).
[17] M. K. Scheller and L. S. Cederbaum, J. Chem. Phys. **100**, 8943 (1994).
[18] T. Sommerfeld, M. K. Scheller, and L. S. Cederbaum, J. Phys. Chem. **98**, 8914 (1994).
[19] V. G. Zakrzewski and J. V. Ortiz, J. Chem. Phys. **102**, 294 (1995).
[20] M. Gutowski, A. I. Boldyrev, J. V. Ortiz, and J. Simons, J. Am. Chem. Soc. **116**, 9262 (1994); J. Rak, M. Gutowski, P. Dokurno, H. V. Thanh, and J. Blazejowski, J. Chem. Phys. **100**, 5810 (1994); M. Gutowski, J. Rak, P. Dokurno, and J. Blazejowski, J. Phys. Chem. **98**, 6280 (1994); M. Gutowski, J. Rak, P. Dokurno, and J. Blazejowski, Inorg. Chem. **33**, 6187 (1994).
[21] T. Sommerfeld, M. K. Scheller, and L. S. Cederbaum, J. Chem. Phys. **103**, 1057 (1995); **104**, 1464 (1996).
[22] M. Gutowski, A. I. Boldyrev, J. Simons, J. Rak, and J. Blazejowski, J. Am. Chem. Soc. **118**, 1173 (1996).
[23] M. L. Mckee, J. Phys. Chem. **100**, 3473 (1996).
[24] D. Mathur, V. R. Bhardwaj, F. A. Rajgara, and C. P. Safvan, Chem. Phys. Lett. **277**, 558 (1997).
[25] T. Sommerfeld, U. V. Riss, H.-D. Meyer, and L. S. Cederbaum, Phys. Rev. Lett. **79**, 1237 (1997).
[26] H. B. Pedersen, N. Djuric, M. J. Jensen, D. Kella, C. P. Safvan, L. Vejby-Christensen, and L. H. Andersen, Phys. Rev. Lett. **81**, 5302 (1998).
[27] T. Sommerfeld and M. S. Child, J. Chem. Phys. **110**, 5670 (1999).
[28] E. Miyoshi and Y. Sakai, J. Chem. Phys. **89**, 7363 (1988); E. Miyoshi, Y. Sakai, A. Murakami, H. Iwaki, H. Terashima, T. Shoda, and T. Kawaguchi, *ibid.* **89**, 4193 (1988).
[29] C. Jin, R. L. Hettich, R. N. Compton, A. Tuinman, A. Derecskei-Kovacs, D. S. Marynick, and B. I. Dunlap, Phys. Rev. Lett. **73**, 2821 (1994).
[30] R. N. Compton, A. A. Tuinman, C. E. Klots, M. R. Pederson, and D. C. Patton, Phys. Rev. Lett. **78**, 4367 (1997).

[31] O. V. Boltalina, P. Hvelplund, M. C. Larsen, and M. O. Larson, Phys. Rev. Lett. **80**, 5101 (1998).
[32] T. Blades and P. Kebarle, J. Am. Chem. Soc. **116**, 10761 (1994); A. T. Blades, J. S. Klassen, and P. Kebarle, *ibid.* **117**, 10563 (1995); T. Blades, Y. Ho, and P. Kebarle, J. Phys. Chem. **100**, 2443 (1996).
[33] M. Yamashita and J. B. Fenn, J. Phys. Chem. **88**, 4451 (1984); **88**, 4671 (1984); J. B. Fenn, M. Mann, C. K. Meng, S. F. Wong, and C. M. Whitehouse, Science **246**, 64 (1989).
[34] G. Khairallah and J. B. Peel, Chem. Phys. Lett. **296**, 545 (1998); J. Phys. Chem. A **101**, 6770 (1997); Chem. Phys. Lett. **268**, 218 (1997).
[35] A. A. Tuinman and R. N. Compton, J. Phys. Chem. A **102**, 9191 (1998).
[36] T. C. Lau, J. Wang, R. Guevremont, and K. W. M. Siu, J. Chem. Soc. Chem. Commun. **1994**, 1487; **1995**, 877.
[37] L. S. Wang, C. F. Ding, X. B. Wang, and S. E. Barlow, Rev. Sci. Instrum. **70**, 1957 (1999).
[38] X. B. Wang, C. F. Ding, and L. S. Wang, Phys. Rev. Lett. **81**, 3551 (1998).
[39] L. S. Wang, C. F. Ding, X. B. Wang, and J. B. Nicholas, Phys. Rev. Lett. **81**, 2667 (1998).
[40] C. F. Ding, X. B. Wang, and L. S. Wang, J. Phys. Chem. A **102**, 8633 (1998).
[41] C. F. Ding, X. B. Wang, and L. S. Wang, J. Chem. Phys. **110**, 3635 (1999).
[42] X. B. Wang, C. F. Ding, J. B. Nicholas, D. A. Dixon, and L. S. Wang, J. Phys. Chem. A **103**, 3423 (1999).
[43] X. B. Wang, C. F. Ding, and L. S. Wang, Chem. Phys. Lett. **307**, 391 (1999).
[44] M. R. Bray, R. J. Deeth, V. J. Paget, and P. D. Sheen, Int. J. Quantum Chem. **61**, 85 (1996).
[45] F. A. Cotton and G. Wilkinson, *Advanced Inorganic Chemistry* (Wiley, New York, 1988).
[46] H. C. Gardner and J. K. Kochi, J. Am. Chem. Soc. **97**, 1855 (1975); J. Y. Chen and J. K. Kochi, *ibid.* **99**, 1450 (1977); C. L. Wong and J. K. Kochi, *ibid.* **101**, 5593 (1979).
[47] C. J. Doona and D. M. Stanbury, Inorg. Chem. **35**, 3210 (1996); M. C. Ghosh, S. Mandal, S. K. Chandra, and E. S. Gould, *ibid.* **34**, 509 (1995); M.-L. Hung, M. L. McKee, and D. M. Stanbury, *ibid.* **33**, 5108 (1994).
[48] R. Jimenez, M. M. Graciani, A. Rodriguez, M. L. Moya, M. F. Sanchez, and P. Lopez-Cornejo, Langmuir **13**, 187 (1997).
[49] P. A. Lay and H. Taube, Inorg. Chem. **28**, 3561 (1989); K. Dehnicke, U. Muller, and R. Weber, *ibid.* **23**, 2563 (1984); R. H. Magnuson, *ibid.* **23**, 387 (1984).
[50] Q. Li, Z. Chen, X. Zheng, and Z. Jin, J. Phys. Chem. **96**, 5959 (1992); G. B. Shulpin, G. V. Nizova, and A. E. Shilov, J. Chem. Soc. Chem. Commun. **1983**, 672.
[51] S. A. Macgregor and K. H. Moock, Inorg. Chem. **37**, 3284 (1998).
[52] T. P. Sleight and C. R. Hare, J. Phys. Chem. **72**, 2207 (1968).
[53] A. J. McCaffery, M. D. Rowe, and D. A. Rice, J. Chem. Soc., Dalton Trans. **1973**, 1605.
[54] L. E. Cox and D. M. Hercules, J. Electron Spectrosc. Relat. Phenom. **1**, 193 (1973).
[55] E. E. Kim, K. Eriks, and R. Magnuson, Inorg. Chem. **23**, 393 (1984).
[56] F. A. Cotton and C. B. Harris, Inorg. Chem. **6**, 376 (1967).
[57] A. Goursot, H. Chermette, and C. Daul, Inorg. Chem. **23**, 305 (1984).
[58] R. J. Deeth and H. D. B. Jenkins, J. Phys. Chem. A **101**, 4793 (1997).
[59] F. A. Cotton, *Chemical Applications of Group Theory* (Wiley, New York, 1971).
[60] G. Herzberg, *Molecular Spectra and Molecular Structure*. III. *Electronic Spectra and Electronic Structure of Polyatomic Molecules* (Van Nostrand Reinhold, New York, 1966).
[61] B. Bersuker, *The Jahn-Teller Effect and Vibronic Interactions in Modern Chemistry* (Plenum, New York, 1984).
[62] S. M. Caseym and D. G. Leopold, J. Phys. Chem. **97**, 816 (1993); X. B. Wang, C. F. Ding, and L. S. Wang, J. Chem. Phys. **110**, 8217 (1999).
[63] N. Bartlett, Angew. Chem. Int. Ed. Engl. **7**, 433 (1968).